

Original Article

The contributions of apoplastic, symplastic and gas phase pathways for water transport outside the bundle sheath in leaves

Thomas N. Buckley

*IA Watson Grains Research Centre, Faculty of Agriculture and Environment, The University of Sydney, Narrabri, New South Wales 2390, Australia***ABSTRACT**

Water movement from the xylem to stomata is poorly understood. There is still no consensus about whether apoplastic or symplastic pathways are more important, and recent work suggests vapour diffusion may also play a role. The objective of this study was to estimate the proportions of hydraulic conductance outside the bundle sheath contributed by apoplastic, symplastic and gas phase pathways, using a novel analytical framework based on measurable anatomical and biophysical parameters. The calculations presented here suggest that apoplastic pathways provide the majority of conductance outside the bundle sheath under most conditions, whereas symplastic pathways contribute only a small proportion. The contributions of apoplastic and gas phase pathways vary depending on several critical but poorly known or highly variable parameters namely, the effective Poiseuille radius for apoplastic bulk flow, the thickness of cell walls and vertical temperature gradients within the leaf. The gas phase conductance should increase strongly as the leaf centre becomes warmer than the epidermis – providing up to 44% of vertical water transport for a temperature gradient of 0.2 K. These results may help to explain how leaf water transport is influenced by light absorption, temperature and differences in leaf anatomy among species.

Key-words: apoplast; leaf hydraulic conductance; stomata; transpiration stream.

INTRODUCTION

Plant water transport and stomatal regulation depend strongly on the distribution of hydraulic resistance and water potential along the transpiration stream. This distribution is somewhat well characterized within stem and leaf xylem, but it remains poorly understood for the pathways taken by water after exiting the xylem in the leaf. Questions that are linked to water flow outside the xylem and remain largely unanswered include: what pathways are taken by water after it exits the bundle sheath surrounding the xylem, where does the bulk of evaporation occur in the leaf, what are the mechanisms by

which light, temperature and dehydration cause changes in the outside-xylem component (K_{ox}) of leaf hydraulic conductance (K_{leaf}), to what degree are different leaf tissues hydraulically coupled to one another, and perhaps most compellingly, how do stomata sense and respond to changes in water supply and evaporative demand?

The prevailing viewpoint that has guided most investigations into these questions assumes that K_{leaf} , calculated as the ratio of water flow to difference in water potential between the petiole water source and bulk leaf tissues, represents a series of liquid phase pathways: through the xylem, then through the bundle sheath and finally through the mesophyll and/or epidermis via apoplastic and/or symplastic routes (Tyree *et al.* 1999; Zwieniecki *et al.* 2007). The apoplastic pathway is often implicitly assumed to be dominated by bulk flow rather than by molecular diffusion of water (Strugger 1943, Tanton & Crowdy 1972, Byott & Sheriff 1976, Evert *et al.* 1985, but see Canny 1990). The possibility that symplastic diffusion may be important in outside-xylem water flow was enhanced by discovery of aquaporins (Agre *et al.* 1993; Chrispeels & Agre 1994), and by experiments demonstrating accumulation of tracers at the proximal margin of living cells adjoining the xylem (Canny 1986), which strongly indicated symplastic flow of water. As a result, suspicion has grown in recent decades that much or most flow outside the xylem may be symplastic (Tyree *et al.* 1981, 1999; Sack *et al.* 2005). The notion that leaf water flow should be strongly limited by high-resistance liquid phase pathways for water diffusion outside the xylem, whether apoplastic or symplastic, was further advanced by Brodribb *et al.* (2007), who showed a strong inverse correlation between K_{leaf} and the pathlength for liquid phase water flow from xylem to stomata.

The intercellular air spaces can also provide a conduit for water transport outside the xylem, although this pathway has received relatively little attention. Boyer (1985), commenting on data of Farquhar & Raschke (1978) showing that the pathlength for vapour diffusion from the sites of evaporation to stomata was roughly half that for helium diffusion across an amphistomatous leaf, noted that this suggested sites of evaporation were deep within the leaf and close to the vascular system. He also noted the apparently high resistance to long-distance water flow in the mesophyll and concluded that most water transport outside the vascular bundles may

Correspondence: T. N. Buckley. Fax: +61 2 6799 2239; e-mail: t.buckley@sydney.edu.au

occur in the vapour phase. This contradicts the prevailing but tacit assumption that the air spaces within the leaf do not represent a physiologically significant pathway for water delivery to the tissues outside the xylem. The notion was not pursued further until Pieruschka *et al.* (2010) and Peak & Mott (2011) suggested that vapour transport between mesophyll and epidermal tissues may play a role in the regulation of stomatal movements. More recently, Rockwell *et al.* (2014) explored the competition between liquid and gas phase water transport in the leaf, focusing on the role of thermal energy transport. That study provided strong theoretical support for the notion that gas phase transport can help deliver water to cells in the vicinity of the stomatal complex.

The pathways for water movement outside the bundle sheath thus remain uncertain, yet knowledge of those pathways is more important than ever, in light of growing awareness of their implications – for example, for interpretation of K_{leaf} in relation to leaf anatomy and environment (Tyree *et al.* 1999; Brodribb *et al.* 2007; Cochard *et al.* 2007; Scoffoni *et al.* 2008), patterns of isotopic enrichment (Barbour & Farquhar 2004) and stomatal behaviour (Buckley 2005; Kaiser & Legner 2007; Peak & Mott 2011). The overarching goal of the present study was to place hypotheses about restrictions on leaf water flow outside the xylem on an explicitly anatomical and biophysical basis. More specifically, the objectives of this paper were (1) to derive a flexible analytical framework for computing the conductances of alternative pathways for water transport from the bundle sheath to stomata (gas phase, symplastic and apoplastic), given the values for measurable anatomical and biophysical parameters; (2) to use this framework to estimate the relative contributions of each pathway to total conductance for horizontal and vertical water movement through various tissues; and (3) to determine which parameters are most important for partitioning flow among pathways.

METHODS

Overview of approach

The approach of this paper will be to derive expressions for the molar conductivities of water movement in different pathways, then to derive expressions for molar conductances in each pathway for different flow directions and tissue types, and finally to apply parameter estimates to the latter expressions to estimate how conductance is partitioned among pathways. Conductivities are derived in the following section, and then scaled to conductances in Appendix 1, using parameter values estimated in Appendix 2 and the generic model of leaf anatomy shown in Fig. 1.

Molar conductivities of alternative pathways for water outside the bundle sheath

This analysis will consider four alternative pathways, or mechanisms, for water movement to the vicinity of stomatal pores after exiting the bundle sheath: liquid diffusion through the symplast, liquid diffusion through the apoplast, liquid

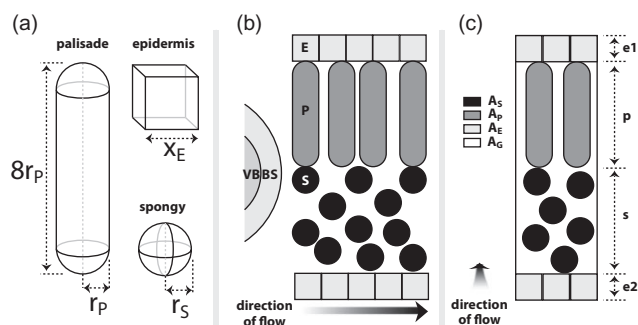


Figure 1. Diagram illustrating the geometry assumed in calculating conductances of alternative water pathways away from the bundle sheath. (a) Geometry of cell types; r_p , r_s and x_E are palisade mesophyll radius, spongy mesophyll radius and epidermal cell length, respectively. (b) Diagram of a transverse section parallel to the direction of water flow away from the bundle sheath (BS), with epidermis (E) and palisade (P) and spongy (S) mesophyll labelled. This is the overall flow path for which relative conductances are calculated in this paper. (c) Diagram of a transverse section normal to the direction of water flow away from the bundle sheath; this is the view ‘seen’ by water. Total areas of each cell type (A_S , A_P and A_E ; spongy, palisade and epidermis, respectively) and of the gas phase pathway (A_G) correspond to the total areas of each colour given in the legend of panel c. Values shown at right represent tissue thicknesses; tissue thickness fractions are: z_E (epidermis) = $(e1+e2)/(e1+e2+p+s)$, z_P (palisade) = $p/(e1+e2+p+s)$ and z_S (spongy) = $s/(e1+e2+p+s)$.

bulk flow through the apoplast and gas diffusion through the intercellular air spaces. This section presents derivations of generic expressions for the molar conductivities of each path (water flow per unit cross-sectional area of flow, per unit time, per unit difference in water potential; $\text{mol m}^{-2} \text{s}^{-1} \text{Pa}^{-1}$). Each conductivity is based, either implicitly or explicitly, on a finite pathlength for water movement. In the expressions derived below, membrane conductivity applies to movement across a single membrane; transcellular and apoplastic conductivities apply to movement across or around a single cell; and gas phase conductivity applies to an arbitrary, generic pathlength. In Appendix 1, these conductivities are scaled to whole-tissue conductances based on estimates of leaf anatomical dimensions.

Symplastic diffusion

Water travelling symplastically will encounter two sets of membranes per cell, and it will also have to diffuse across the interior of cell. Each membrane has an osmotic water permeability of P_m (m s^{-1} ; equivalently, $\text{m}^3 \text{m}^{-2} \text{s}^{-1}$). The molar flux through one membrane, J_m ($\text{mol m}^{-2} \text{s}^{-1}$) is

$$J_m = \frac{P_m}{RT} \Delta\psi \quad (1)$$

where $\Delta\psi$ is the water potential difference across the membrane (Pa), R is the gas constant ($8.3144621 \text{ Pa m}^3 \text{ mol}^{-1}$) and T is temperature in kelvins. (A list of mathematical symbols is given in Table 1.) The molar hydraulic conductivity, k_m

Table 1. List of mathematical quantities that appear in this paper

Description	Symbol	Units
Cross-sectional area of apoplast	A_a	m^2
Total area available for horizontal transport	A_H	m^2
Area available for horizontal transport in tissue j	A_{Hj}	m^2
Total area available for vertical transport	A_V	m^2
Area available for vertical transport in tissue j	A_{Vj}	m^2
Water vapour concentration	c	$mol\ m^{-3}$
Water vapour concentration at vascular plane	c_1	$mol\ m^{-3}$
Water vapour concentration near stomata	c_2	$mol\ m^{-3}$
Water vapour concentration difference	Δc	$mol\ m^{-3}$
Saturated water vapour concentration	c_s	$mol\ m^{-3}$
Saturated water vapour concentration at vascular plane	c_{s1}	$mol\ m^{-3}$
Saturated water vapour concentration near stomata	c_{s2}	$mol\ m^{-3}$
Molecular diffusivity of water vapour in air	D_{wa}	$m^2\ s^{-1}$
Molecular diffusivity of liquid water in water	D_{ww}	$m^2\ s^{-1}$
Apoplastic bulk flow around one cell	F_{aB}	$mol\ s^{-1}$
Fraction of mesophyll surface area that adjoins other cells	f_c	–
Dynamic viscosity of water	η	Pa s
Water vapour flux in intercellular air spaces	J_g	$mol\ m^{-2}\ s^{-1}$
Water flux into one cell	J_m	$mol\ m^{-2}\ s^{-1}$
Total conductivity of apoplast	k_a	$mol\ m^{-2}\ s^{-1}\ Pa^{-1}$
Conductivity of apoplast for bulk flow	k_{aB}	$mol\ m^{-2}\ s^{-1}\ Pa^{-1}$
Conductivity of apoplast for diffusive transport	k_{aD}	$mol\ m^{-2}\ s^{-1}\ Pa^{-1}$
Conductivity of cell interior for one cell	k_c	$mol\ m^{-2}\ s^{-1}\ Pa^{-1}$
Isothermal conductivity of gas phase pathway	k_g	$mol\ m^{-2}\ s^{-1}\ Pa^{-1}$
Anisothermal conductivity of gas phase pathway	k'_g	$mol\ m^{-2}\ s^{-1}\ Pa^{-1}$
Conductivity of one cell membrane	k_m	$mol\ m^{-2}\ s^{-1}\ Pa^{-1}$
Conductance for horizontal apoplastic flow around a cell of type j	K_{aHj}	$mol\ s^{-1}\ Pa^{-1}$
Conductance for vertical apoplastic flow around a cell of type j	K_{aVj}	$mol\ s^{-1}\ Pa^{-1}$
Conductance for horizontal flow through the interior of a cell of type j	K_{cHj}	$mol\ s^{-1}\ Pa^{-1}$
Conductance for vertical flow through the interior of a cell of type j	K_{cVj}	$mol\ s^{-1}\ Pa^{-1}$
Total conductance for horizontal gas phase flow in tissue type j	K_{gasHj}	$mol\ s^{-1}\ Pa^{-1}$
Total conductance for vertical gas phase flow in tissue type j	K_{gasVj}	$mol\ s^{-1}\ Pa^{-1}$
Leaf hydraulic conductance	K_{leaf}	$mol\ m^{-2}\ s^{-1}\ Pa^{-1}$
Conductance for horizontal entry into a cell of type j	K_{mHj}	$mol\ s^{-1}\ Pa^{-1}$
Conductance for vertical entry into a cell of type j	K_{mVj}	$mol\ s^{-1}\ Pa^{-1}$
Leaf hydraulic conductance outside xylem	K_{ox}	$mol\ m^{-2}\ s^{-1}\ Pa^{-1}$
Total conductance for horizontal symplastic flow in tissue type j	K_{symHj}	$mol\ s^{-1}\ Pa^{-1}$
Total conductance for vertical symplastic flow in tissue type j	K_{symVj}	$mol\ s^{-1}\ Pa^{-1}$
Permeability of apoplast for bulk flow (used in Darcy's Law)	κ	m^2
Length of path across one cell interior	l_c	m
Length of gas phase pathway	l_g	m
Total horizontal liquid phase pathlength	l_{LH}	m
Total vertical liquid phase pathlength in tissue j	l_{LVj}	m
Number of Poiseuille conduits in apoplast area A_a	m	–
Number of cells in horizontal liquid phase flow path of tissue j	n_{Hj}	–
Number of cells in vertical liquid phase flow path of tissue j	n_{Vj}	–
Water vapour pressure	p	Pa
Hydrostatic pressure difference apoplastic flow path	ΔP	Pa
Porosity of cell walls	p_a	–
Total pressure of air in intercellular air spaces	p_i	Pa
Osmotic water permeability of cell membranes	p_m	$m\ s^{-1}$
Palisade mesophyll tissue porosity	p_P	–
Spongy mesophyll tissue porosity	p_S	–
Saturated water vapour pressure	p_{sat}	Pa
Saturated water vapour pressure at vascular plane	p_{sat1}	Pa
Saturated water vapour pressure near stomata	p_{sat2}	Pa
Gas constant	R	$Pa\ m^3\ mol^{-1}\ K^{-1}$
Effective Poiseuille radius of cell wall bulk flow paths	R_a	m
Palisade mesophyll cell radius	r_P	m
Spongy mesophyll cell radius	r_S	m
Absolute temperature	T	K
Absolute temperature at vascular plane	T_1	K
Absolute temperature near stomata	T_2	K
Temperature difference between vascular plane and stomata	ΔT	K
Cell wall thickness	t_a	m
Tortuosity of flow pathways through cell walls	τ_a	–
Celsius temperature	T_c	$^{\circ}C$
Molar volume of water	V_w	$m^3\ mol^{-1}$
Water vapour mole fraction	w	$mol\ mol^{-1}$
Saturated water vapour mole fraction	w_s	$mol\ mol^{-1}$
Epidermal cell width	x_E	m
Ratio of apoplastic to transcellular pathlength	y	–
Water potential at vascular plane	ψ_1	Pa
Water potential near stomata	ψ_2	Pa
Water potential difference	$\Delta\psi$	Pa
Fraction of leaf thickness occupied by tissue j	z_j	–

Nominal values and ranges for parameters that varied in sensitivity analyses are given in Table 2. The generic subscript j is a placeholder for tissue type (j = E, P or S for epidermis, palisade mesophyll and spongy mesophyll, respectively). Note: area units for K_{leaf} and K_{ox} represent leaf area, whereas area units for conductivities represent cross-sectional areas of flow paths.

($\text{mol m}^{-2} \text{s}^{-1} \text{Pa}^{-1}$), is the flux divided by the water potential gradient, or

$$k_m = \frac{P_m}{RT}. \quad (2)$$

The effective permeability for the diffusive path across the cell interior equals the diffusion coefficient for water in water, D_{ww} ($\text{m}^2 \text{s}^{-1}$), divided by the pathlength across the cell in the direction of flow, l_c (m), so the molar hydraulic conductivity for diffusion across the interior of one cell, k_c , is

$$k_c = \frac{D_{ww}}{l_c RT}. \quad (3)$$

Apoplastic diffusion

An apoplastic route will flow along the cell walls forming the perimeter around each cell in the symplastic pathway. The molar conductivity for water diffusion along this pathway, k_{aD} , is similar to that for the cell interior in the symplastic route. However, in the apoplast, the conductivity must be modified in two ways: (1) the conductivity must be multiplied by a factor p_a/τ_a to account for the porosity p_a of the cell wall (void fraction, which is less than 1) and the tortuosity τ_a of the water paths through those voids (the ratio of actual mean path length to the shortest possible path length; this ratio is greater than 1); and (2) the pathlength l_c must be multiplied by a factor γ (unitless) to account for the fact that the pathlength around a cell may be greater than that directly across the cell. (γ depends on cell geometry; see Appendix 1.) For an apoplastic route spanning one cell, k_{aD} is thus

$$k_{aD} = \frac{p_a D_{ww}}{\tau_a \gamma l_c RT}. \quad (4)$$

Apoplastic bulk flow

Bulk flow through the apoplast, F_{aB} (mol s^{-1}), can be described using Darcy's Law:

$$F_{aB} = \frac{\kappa A_a}{\eta \gamma l_c V_w} \Delta P \quad (5)$$

where κ is the intrinsic permeability of the cell wall (m^2), A_a is the total apoplastic cross-sectional flow area, ΔP (Pa) is the difference in hydrostatic pressure in the apoplast across the effective flow path, η is the dynamic viscosity (Pa s), V_w is the molar volume of water ($\text{m}^3 \text{mol}^{-1}$) and γl_c is the apoplastic pathlength around the cell. The permeability κ can be estimated by analogy to the Hagen-Poiseuille equation, which describes laminar bulk flow through cylindrical tubes. Assuming that the area of the apoplast available for flow can be modelled as a number m of conduits of radius R_a , the Poiseuille flow rate is

$$F_{aB} = \frac{m \pi R_a^4}{8 \eta \tau_a \gamma l_c V_w} \Delta P \quad (6)$$

which accounts for the tortuosity (τ_a) of cell wall flow paths, as in Eqn 4. The number of conduits is computed by setting

the total conduit area, $m \pi R_a^2$, equal to the total cell wall void area, which is the product of the porosity p_a and total apoplast cross-sectional area A_a . Thus, $m \pi R_a^2 = p_a A_a$, or $m \pi R_a^4 = p_a A_a R_a^2$, so

$$F_{aB} = \frac{p_a A_a R_a^2}{8 \eta \tau_a \gamma l_c V_w} \Delta P. \quad (7)$$

Assuming osmotic gradients in the apoplast water are negligible, $\Delta P \approx \Delta \psi$. The apoplastic bulk flow conductivity k_{aB} is the flow divided by the gradient $\Delta \psi$ and by the flow area A_a , or

$$k_{aB} = \frac{p_a R_a^2}{8 \eta \tau_a \gamma l_c V_w}. \quad (8)$$

Because diffusion and advection (bulk flow) are additive, k_{aD} and k_{aB} can be combined into a single term for the molar hydraulic conductivity of the apoplast, k_a :

$$k_a = \frac{p_a}{\tau_a \gamma l_c} \left(\frac{D_{ww}}{RT} + \frac{R_a^2}{8 \eta V_w} \right). \quad (9)$$

Gas phase diffusion

The intercellular air spaces represent a conduit through which water can move outside the bundle sheath, in precisely the same sense that the adjacent cells and cell walls are conduits. Thus, gas phase water transport can increase the total conductance for water transport outside the bundle sheath, so it can also affect the water potential at any particular point outside the bundle sheath. A consequence of this fact is that the quantity described as 'leaf hydraulic conductance' may include a gas phase component. However, because the word 'hydraulic' is generally reserved for properties involving liquid water, this word should be omitted when describing the gas phase component.

It is important to recognize that a molar conductivity for vapour flux can be defined and calculated in precisely the same terms as for liquid water fluxes. For liquids, molar hydraulic conductivities were defined earlier as ratios of molar fluxes (with units of $\text{mol m}^{-2} \text{s}^{-1}$) to water potential gradients (with units of Pa). Although gas flux is conventionally described in terms of gradients in concentration, partial pressure or mole fraction, water vapour concentrations can also be expressed as water potential gradients, as shown below. To compute the molar conductivity for gas phase transport within the leaf, one can begin with Fick's first law of diffusion,

$$J_g = D \frac{dc}{dx} \approx \frac{D_{wa}}{l_g} \Delta c \quad (10)$$

where J_g is the water vapour flux (subscript g for gas phase) ($\text{mol m}^{-2} \text{s}^{-1}$), D_{wa} is the molecular diffusivity of water vapour in air ($\text{m}^2 \text{s}^{-1}$), l_g is the length of the gas phase flow pathway (m) and Δc is the difference in water vapour concentration (mol m^{-3}) across that pathway. To relate concentration to water potential, it is useful to first relate water potential to water vapour mole fraction (w , mol mol^{-1}), and then to relate w to concentration. The relationship between water potential (ψ) and w is

$$\psi = \frac{RT}{V_w} \ln \frac{w}{w_s} \approx \frac{RT}{V_w} \left(\frac{w}{w_s} - 1 \right) \quad (11)$$

where w_s is the saturation water vapour mole fraction of air at a temperature T (kelvins) (Nobel 1991). The approximate equality on the right hand side of Eqn 11 uses $\ln(x) \approx x - 1$ for $x \approx 1$, which results in an error of less than 1% for water potential at the evaporating site above -2.2 MPa and temperature between 0 and 40 °C (not shown). To relate w and w_s to water vapour concentrations, note that $w = p/P_i$, where p is vapour pressure (Pa) and P_i is total pressure of the intercellular air (Pa). The ideal gas law ($p = cRT$) then implies $w/w_s = [cRT/P_i]/[c_sRT/P_i] = c/c_s$, where c_s is the value of c at saturation. This gives

$$\psi \approx \frac{RT}{V_w} \left(\frac{c}{c_s} - 1 \right). \quad (12)$$

Therefore, $\Delta\psi \approx \Delta c(RT/V_w c_s)$, provided temperature does not vary along the flow path (this assumption will be relaxed below). Solving this for Δc and applying the result to 10 gives

$$J_g = \frac{D_{wa} V_w c_s}{l_g RT} \Delta\psi. \quad (13)$$

Finally, replacing c_s with p_{sat}/RT , where p_{sat} is the saturation vapour pressure, and dividing the flux by the water potential gradient $\Delta\psi$ gives the isothermal molar conductivity of the gas phase pathway to water vapour, k_g (mol m⁻² s⁻¹ Pa⁻¹), as

$$k_g = \frac{D_{wa} V_w p_{sat}}{l_g (RT)^2}. \quad (14)$$

It can be shown (see Appendix 3) that, if a vertical temperature gradient occurs between the vascular plane and the epidermal plane (i.e. near stomata), then the ratio of flux to water potential gradient between those two planes becomes

$$k'_g = k_g(T_1) + \frac{D_{wa}}{l_g R \Delta\psi} \left(\frac{p_{sat1}}{T_1} - \frac{p_{sat2}}{T_2} \right) \left(\frac{V_w \psi_2}{RT_1} + 1 \right) \quad (15)$$

where the subscripts 1 and 2 refer to the conditions near the vertical centre of the leaf and near the epidermis,

respectively, l_g is the distance between those two locations, $k_g(T_1)$ means k_g evaluated at T_1 , and $\Delta\psi = \psi_1 - \psi_2$. Equation 15 is a general (not isothermal) expression for the molar conductivity for intercellular water vapour diffusion. Although this expression has somewhat limited utility because one must supply values of $\Delta\psi$, T_1 and T_2 , it can nevertheless be used to assess the effect of temperature gradients on gas transport within leaves. In the Results section, Eqns 14 and 15 will be compared at several values for $\Delta\psi$ and across a range of values for the difference between T_1 and T_2 (expressed below as $\Delta T = T_1 - T_2$).

Simulation procedures

For each tissue type (epidermis, palisade mesophyll and spongy mesophyll) and flow direction (horizontal and vertical), the anatomical model illustrated in Fig. 1 was used to scale the conductivities derived above to whole-path conductances, based on the areas available for flow in each pathway, the pathlengths for flow, and for liquid phase pathways, the numbers of cells encountered along the pathway in each case. These calculations are explained in detail in Appendix 1. This resulted in conductance values for three parallel pathways – apoplastic, symplastic and gas phase – within each tissue type and for each flow direction. These three parallel conductances were then summed within each tissue type and flow direction, and each of the three values was expressed as a percentage of the resulting sum. Appendix 2 describes estimation of parameter values required for these calculations, as well as ranges used in parameter sensitivity analysis; the resulting values and ranges are given in Table 2.

To assess the sensitivity of these calculations to variation in parameters other than temperature, key parameters were varied systematically within the limits given in Table 2. The effect of temperature on these calculations was then assessed in two ways: by calculating the effect of uniform variations in temperature between 0 and 40 °C on the conductivities for

Table 2. List of parameters that varied in sensitivity analyses, with nominal values and ranges

Description	Symbol	Units	Nominal value	Range
Fraction of mesophyll surface area that adjoins other cells	f_c	–	0.275	0.15–0.40
Ratio of vertical gas to liquid phase pathlengths (palisade)	l_g/l_{LVP}	–	1.43	0.9–1.96
Ratio of horizontal gas to liquid phase pathlengths (spongy)	$l_g/l_{LH,S}$	–	1.13	0.69–1.57
Ratio of vertical gas to liquid phase pathlengths (spongy)	$l_g/l_{LV,S}$	–	1.13	0.69–1.57
Effective porosity of cell walls	p_a/τ_a	–	0.2	0.1–0.5
Palisade mesophyll tissue porosity	p_P	–	0.19	0.07–0.40
Spongy mesophyll tissue porosity	p_S	–	0.39	0.27–0.63
Osmotic water permeability of cell membranes	P_m	m s ⁻¹	40·10 ⁻⁶	(10–70)·10 ⁻⁶
Effective Poiseuille radius of cell wall bulk flow paths	R_a	m	3·10 ⁻⁹	(1.5–10)·10 ⁻⁹
Palisade mesophyll cell radius	r_P	m	6.5·10 ⁻⁶	(3–10)·10 ⁻⁶
Spongy mesophyll cell radius	r_S	m	12·10 ⁻⁶	(5–19)·10 ⁻⁶
Cell wall thickness	t_a	m	0.3·10 ⁻⁶	(0.2–0.4)·10 ⁻⁶
Epidermal cell width	x_E	m	27·10 ⁻⁶	(11–43)·10 ⁻⁶
Epidermal tissue thickness fraction	z_E	–	0.19	0.05–0.38
Ratio of palisade to spongy tissue thickness fractions	z_P/z_S	–	0.75	0.5–2.0

each flow pathway, and second, by using Eqn 15 to assess how vertical temperature gradients may affect the inferred gas phase conductivity. This required a range of values for the temperature gradient (ΔT) and water potential gradient ($\Delta\psi$) from the vascular plane to the epidermis. Simulations by Rockwell *et al.* (2014) suggested that ΔT could be as large as 0.15 K, and that $\Delta\psi$ could be as large as $0.7 \cdot 10^6$ Pa. The sensitivity analysis presented here assessed the effect of ΔT between 0 and 0.20 K for four values of $\Delta\psi$: 0.1, 0.25, 0.5 and $1.0 \cdot 10^6$ Pa, at three baseline temperatures (5, 25 and 45 °C). Water potential and temperature at the bundle sheath were set to be $-1.5 \cdot 10^6$ Pa and 25 °C, respectively, unless otherwise noted, and nominal values given in Table 2 were used for other parameters. All calculations were performed in Microsoft Excel; the spreadsheet is included as Supporting Information Table S1.

RESULTS

Effects of temperature gradients on gas phase conductivity

Figure 2 shows how the effective gas phase conductivity (k_g' , Eqn 15; the ratio of molar gas flux to water potential gradient) differed from the isothermal gas phase conductivity (k_g , Eqn 14) in relation to the assumed temperature decrease between the vascular plane and the epidermis (ΔT), at three temperatures (Fig. 2a) and for four values of the water potential decrease from the vascular plane to the epidermis (Fig. 2b). For small water potential gradients (0.1 MPa), k_g' was over 16 times greater than k_g at a temperature gradient of 0.2 K. Even for large water potential gradients (1.0 MPa), k_g' was over 2.5 times greater than k_g . The ratio of k_g'/k_g varied by only 2.8% across a wide range of values for the water potential at the bundle sheath (from 0 to -4 MPa), and by only 15% across a range of values for the temperature at the bundle sheath (5 to 45 °C) (not shown), which indicates that the ratio k_g'/k_g is far more sensitive to gradients in temperature and water potential than to the absolute magnitudes of either temperature or water potential.

These results suggest that the isothermal approximation for k_g is not justified when temperature gradients greater than ~ 0.01 K exist between the vascular plane and epidermis. All subsequent calculations were therefore repeated at two values for ΔT (0 and 0.2 K).

Proportions of total conductance in each pathway

Figures 3 and 4 show the calculated proportions of total conductance for each pathway and tissue, for horizontal (Fig. 3) and vertical transport (Fig. 4). Two sets of results are shown in each case, using the nominal value for cell wall thickness of $0.3 \mu\text{m}$ (Figs 3a & 4a,b) and the average value ($1.4 \mu\text{m}$) from a recent survey of 14 species by John *et al.* (2013) (Figs 3b & 4c,d). For vertical transport, these calculations were also repeated assuming a vertical temperature gradient (ΔT) of 0.2 K (Fig. 4b,d).

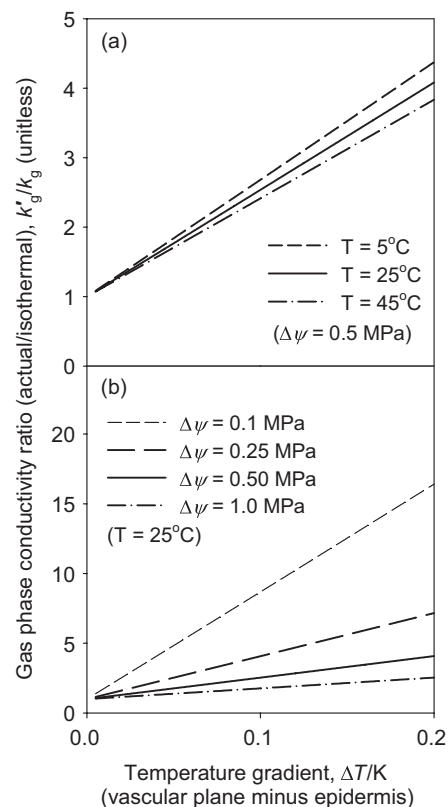


Figure 2. Effect of temperature difference between the vascular plane and the epidermis (ΔT) (the epidermis being cooler) on the ratio of the effective molar conductivity for intercellular vapour diffusion (k_g') to the isothermal value of that conductivity (k_g), at (a) three different baseline temperatures, T , and assuming a water potential decrease of 0.5 MPa from the vascular plane to the epidermis, and (b) four different values of the water potential decrease from the vascular plane to the epidermis, all at a baseline temperature of 25 °C. Note the different vertical axes in (a) and (b).

In the absence of a vertical temperature gradient ($\Delta T = 0$ K) and using the smaller value for cell wall thickness ($0.3 \mu\text{m}$), these calculations suggest that the conductance for water movement outside the bundle sheath is predominantly apoplastic. Apoplastic conductance was 72–88% of the total within each tissue type and flow direction (horizontal flow, Fig. 3a; vertical flow, Fig. 4a,b). The remainder of conductance was contributed in varying proportions by symplastic and gas phase pathways: 5.9% symplastic and 7.3% gas phase for horizontal palisade transport (Fig. 3a), 11.4% symplastic and 13.7% gas phase for vertical palisade transport (Fig. 4a), and 11.6% symplastic and 16.2% gas for both horizontal and vertical spongy transport (Figs 3a & 4a). Using the larger value for cell wall thickness ($1.4 \mu\text{m}$), apoplastic transport was predicted to be even more dominant, contributing over 92% of total conductance in all cases.

When a 0.2 K vertical gradient in temperature was assumed to occur between the vascular plane and the stomata, the predicted contribution of the gas phase pathway to total vertical conductance increased greatly, to 39.2% for

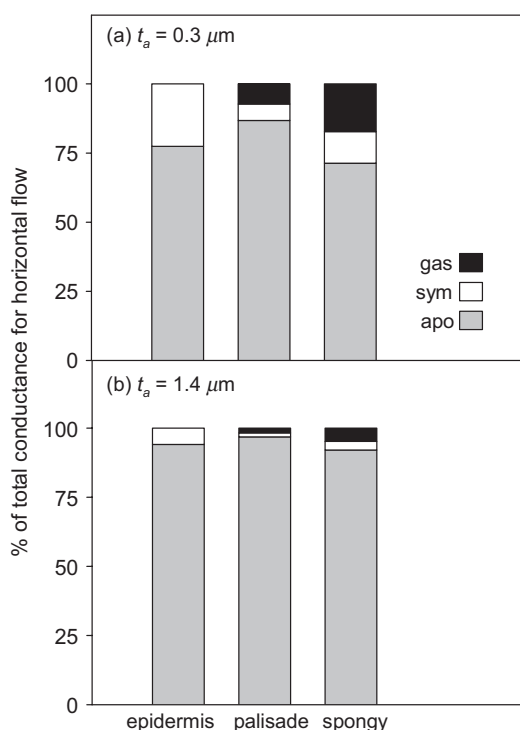


Figure 3. Proportions of molar conductance for horizontal water transport contributed by gas phase, symplastic and apoplastic pathways, in the epidermis, palisade mesophyll and spongy mesophyll. (a) Using the nominal value for cell wall thickness, t_a ($0.3 \mu\text{m}$); (b) using the mean value of cell wall thickness reported in a survey of 14 species by John *et al.* (2013) ($1.4 \mu\text{m}$). Nominal values given in Table 2 were used for other parameters.

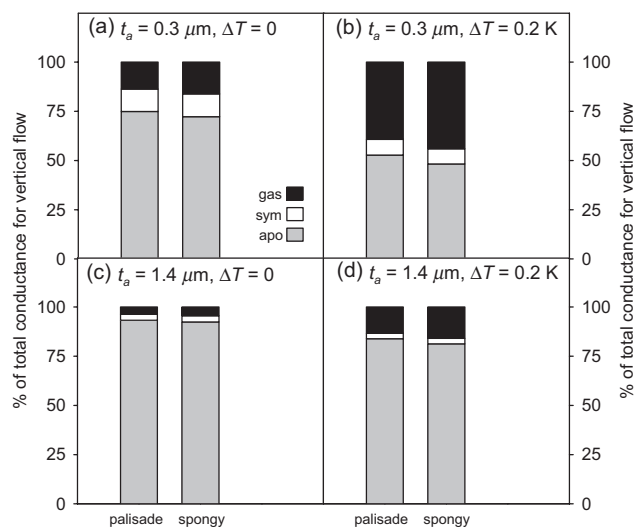


Figure 4. Proportions of molar conductance for vertical water transport contributed by gas phase, symplastic and apoplastic pathways, in the palisade and spongy mesophyll. (a, b) Using the nominal value for cell wall thickness, t_a ($0.3 \mu\text{m}$); (c, d) using the mean value of t_a ($1.4 \mu\text{m}$) reported in a survey of 14 species by John *et al.* (2013). (a, c) Assuming no vertical temperature gradient between the vascular plane and the epidermis; (b, d) assuming a temperature difference of 0.2 K (with the epidermis being cooler). Nominal values given in Table 2 were used for other parameters.

palisade and 44.0% for spongy mesophyll (Fig. 4b). These numbers were somewhat smaller when $\Delta T = 0.2 \text{ K}$ was combined with the larger value for cell wall thickness (Fig. 4d): in this case, gas phase transport was 13.3% of the total for palisade and 15.9% for spongy mesophyll, respectively.

Systematic parameter sensitivity analysis

Due to the large number of input parameters and output variables, only the strongest parameter sensitivities are described here and presented in Figs 5–8. The strongest effect, by far, was that of the effective Poiseuille radius of

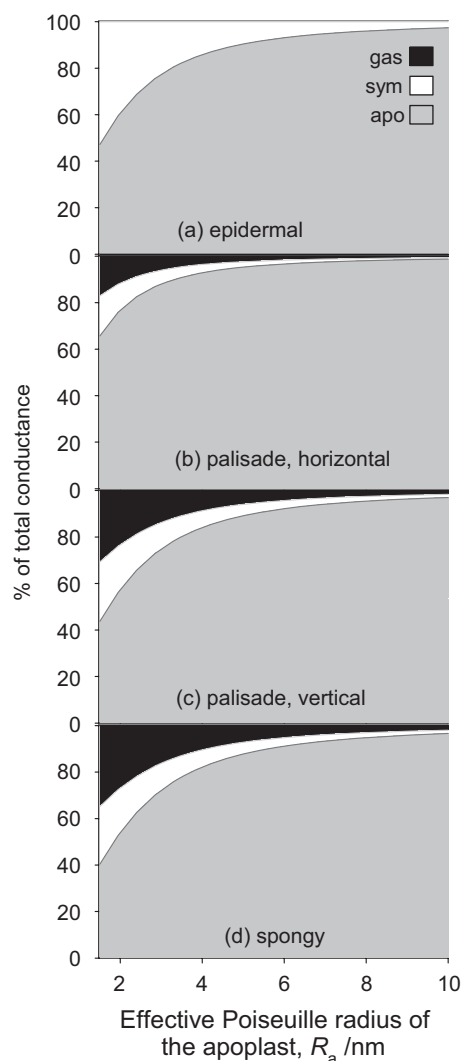


Figure 5. Effect of variation in the effective Poiseuille radius of cell wall bulk flow paths (R_a) on the % of total conductance in gas phase, symplastic and apoplastic pathways for (a) horizontal flow through the epidermis, (b) horizontal flow through the palisade mesophyll, (c) vertical flow through the palisade mesophyll and (d) flow through the spongy mesophyll. (Vertical and horizontal flow are not distinguished for spongy mesophyll because % conductances are identical for both directions in the absence of a vertical temperature gradient.) Nominal parameter values given in Table 2 were used for all other parameters.

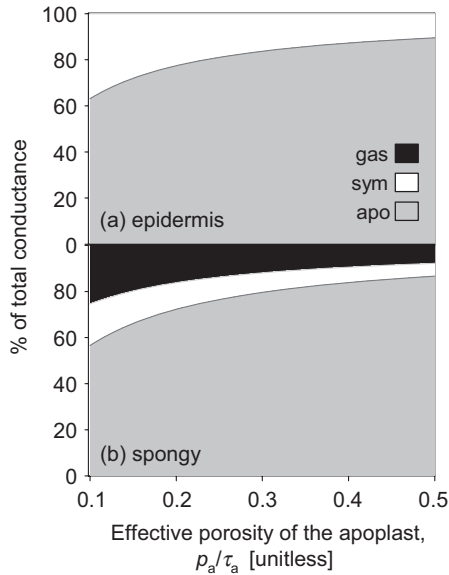


Figure 6. Effect of variation in the effective porosity of the apoplast (p_a/τ_a) on the % of total conductance in gas phase, symplastic and apoplastic pathways for (a) horizontal flow through the epidermis and (b) flow through the spongy mesophyll. Nominal parameter values given in Table 2 were used for all other parameters.

apoplastic bulk flow pathways, R_a . This is due to the dependence of apoplastic bulk flow conductivity (k_{aB}) on the square of R_a (Eqn 8). For example, variation in R_a between 1.5 and 10 μm caused the apoplastic proportions of conductance in the spongy mesophyll to vary by nearly 60% (Fig. 5d). The effective porosity of the apoplast (p_a/τ_a , Fig. 6) also had large effects on the partitioning of conductance among pathways: for example, the contribution of apoplastic pathways to total vertical conductance in the spongy mesophyll increased from 57 to 87% as p_a/τ_a increased from 0.1 to 0.5. Increases in epidermal cell size (x_E , Fig. 7) from 11 to 43 μm caused the apoplastic share of total conductance in the epidermis to decline from 95 to 60%, with a commensurate increase in the symplastic share from 5 to 40%. Finally, increases in spongy

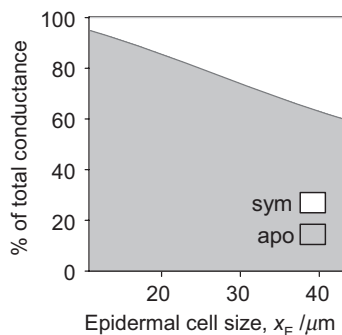


Figure 7. Effect of variation in the size of epidermal cells (x_E) on the % of total conductance in symplastic and apoplastic pathways for horizontal flow through the epidermis. Nominal parameter values given in Table 2 were used for all other parameters.

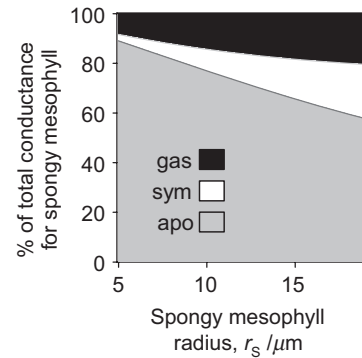


Figure 8. Effect of variation in the radius of spongy mesophyll cells (r_s) on the % of total conductance in symplastic and apoplastic pathways for water flow through the spongy mesophyll. Nominal parameter values given in Table 2 were used for all other parameters.

mesophyll cell radius (r_s , Fig. 8) from 5 to 19 μm caused the apoplastic share of total conductance to decline from 90 to 59% for horizontal transport through the spongy mesophyll, and from 89 to 57% for vertical transport.

Effects of uniform temperature changes on conductivities

Responses of intracellular, apoplastic and gas phase conductivities (k_c , k_a and k_g , respectively) to temperature are shown in Fig. 9a. [The response of membrane conductivity (k_m) is not shown because the effect of temperature on membrane permeability (P_m) in mesophyll cells is not known, yet is likely to be substantial based on measurements in roots (Lee *et al.* 2005; Murai-Hatano *et al.* 2008); see the Discussion section.] The temperature responses of k_c and k_a are similar; the latter response is slightly stronger due to the greater effect of temperature on viscosity (η) than on the molecular diffusivity of water in water (D_{ww}) (Fig. 9b). The temperature response of k_g is much stronger than those of k_c and k_a (Fig. 9a) despite the dependence of k_g on the inverse square of absolute temperature (Eqn 14) and the weaker temperature dependence of the diffusion coefficient for water vapour in air (D_{wa}) as compared with that of D_{ww} . The greater response of k_g to temperature results from its dependence on the saturation vapour pressure (p_{sat}) (Eqn 14).

DISCUSSION

The calculations presented here provide novel insights into the potential contributions of different modes of water transport to flow outside the bundle sheath. Most notably, these calculations predicted that apoplastic transport dominates symplastic transport in most conditions, and that gas phase pathways contributed up to 44% of total conductance for vertical transport. The latter percentage was strongly dependent upon the assumed vertical temperature gradient between the centre of the leaf (the vascular plane) and the epidermis (ΔT): for $\Delta T = 0.2$ K, gas phase conductance was 16–44% of total vertical conductance in the spongy

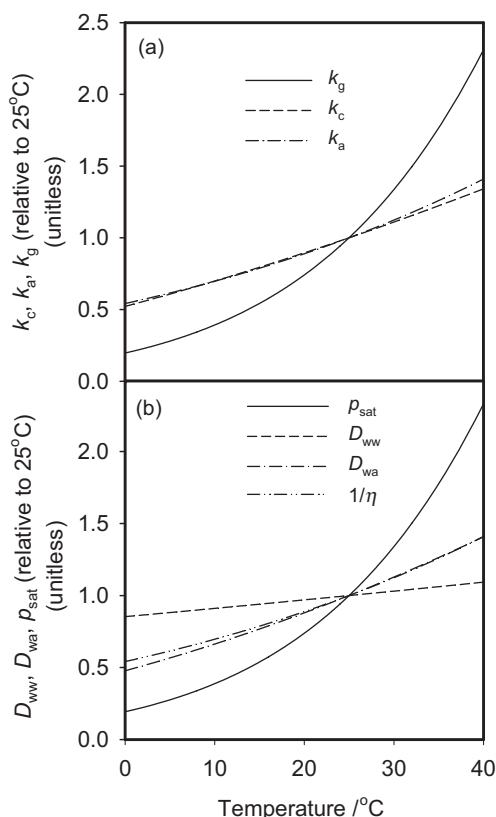


Figure 9. Effect of temperature on factors of hydraulic conductance for water flow away from the bundle sheath. (a) Molar conductivities of the transcellular (k_c), apoplastic (k_a) and gas phase (k_g) pathways. (b) Molecular diffusivity of water in liquid water (D_{ww}); molecular diffusivity of water vapour in air (D_{wa}); saturation water vapour pressure (p_{sat}); and the inverse of dynamic viscosity (η). All values are expressed relative to absolute values at 25 °C.

mesophyll, whereas for $\Delta T = 0$, it was just 4–16% of the total. Although the predicted proportions of total conductance contributed by apoplastic and gas phase pathways varied widely in relation to the values of some key parameters including ΔT , the contribution of symplastic pathways was quite small across a wide range of most parameter values. These calculations suggest the tentative conclusion that symplastic transport does not represent a major restriction for water flow outside the bundle sheath.

Vapour transport in leaves

The possibility that gas phase transport may contribute substantially to water flow in the leaf was suggested by Boyer (1985), and more recently explored in detail by Rockwell *et al.* (2014) in relation to its implications for heat transport and the sites of evaporation within leaves. As noted by the latter authors, if gas phase water transport is significant, then differences in the outside-xylem component (K_{ox}) of leaf hydraulic conductance (K_{leaf}) may partly reflect differences in the properties of gas phase transport. This contrasts with the

traditional conception of leaf water flow, in which water moves from the xylem to sites of evaporation along liquid phase flow paths in order to replace water lost from cells to the intercellular air spaces. Those air spaces are not typically perceived to support a substantial fraction of water flow; indeed, they have usually been viewed as sinks, not sources, for water in adjacent cells. The results presented here suggest that the conductance of gas phase pathways for water transport is large enough to support a significant fraction of water flow through tissues outside the bundle sheath. The gas phase conductance was also predicted to increase dramatically as the leaf interior heats up relative to the epidermis as a result of light absorption. These results, together with the demonstration by Rockwell *et al.* (2014) that thermally driven vapour transfer within the leaf contributes to the apparent value of K_{leaf} , show that the traditional perspective on water movement outside the xylem in leaves clearly needs to be revised to include the intercellular air spaces as an important conduit for water transport.

An interesting feature of the simulations by Rockwell *et al.* (2014) was that, in general, evaporation should occur primarily from either the ‘perivascular’ region (i.e. the bundle sheath or other cells near the vascular bundles) or the ‘peristomatal’ region (i.e. the surfaces of cells lining the substomatal chamber that subtends the stomatal pore), but that very little net evaporation should occur from tissues lining the pathway between those two regions. It can be argued that this should be the case even under isothermal conditions, and that it is simply a result of the fact that the intercellular spaces are a conduit for water transport just as the adjacent tissues are conduits. When the air spaces are viewed in this manner, it becomes apparent that water will generally flow in parallel in the gas and liquid phase pathways until the two pathways converge near the stomatal pore, and that little or no net transfer should necessarily occur between the pathways along the way (i.e. little or no net evaporation or condensation should occur along the way). This is best understood by considering an electrical analog (Fig. 10). If two parallel pathways share the same ‘ground’ (i.e. low-potential sink, which, in the leaf, is the air space below the stomatal pore), they will also share the same gradient of potential along the way, provided the two pathways accumulate resistance steadily with distance (Fig. 10a). As a result, there will in general be no potential differences to drive flow between the pathways (Fig. 10b). In the leaf, this means that the tissues along the flow path will be in a state of dynamic water potential equilibrium with the adjacent air spaces, and that net evaporation will not occur along most of that path. This mirrors one of the conclusions of Rockwell *et al.* (2014), and it suggests that this particular conclusion may be robust to differences in the distribution of radiation absorption: all that matters is that the gas and liquid phase pathways accumulate resistance steadily with distance.

Where will evaporation occur, then, according to this view? It will occur in relation to flow: if 15% of flow occurs as vapour diffusion from near the bundle sheath, then 15% of evaporation will occur from near the bundle sheath. Likewise, if 85% of flow occurs in the liquid phase through the

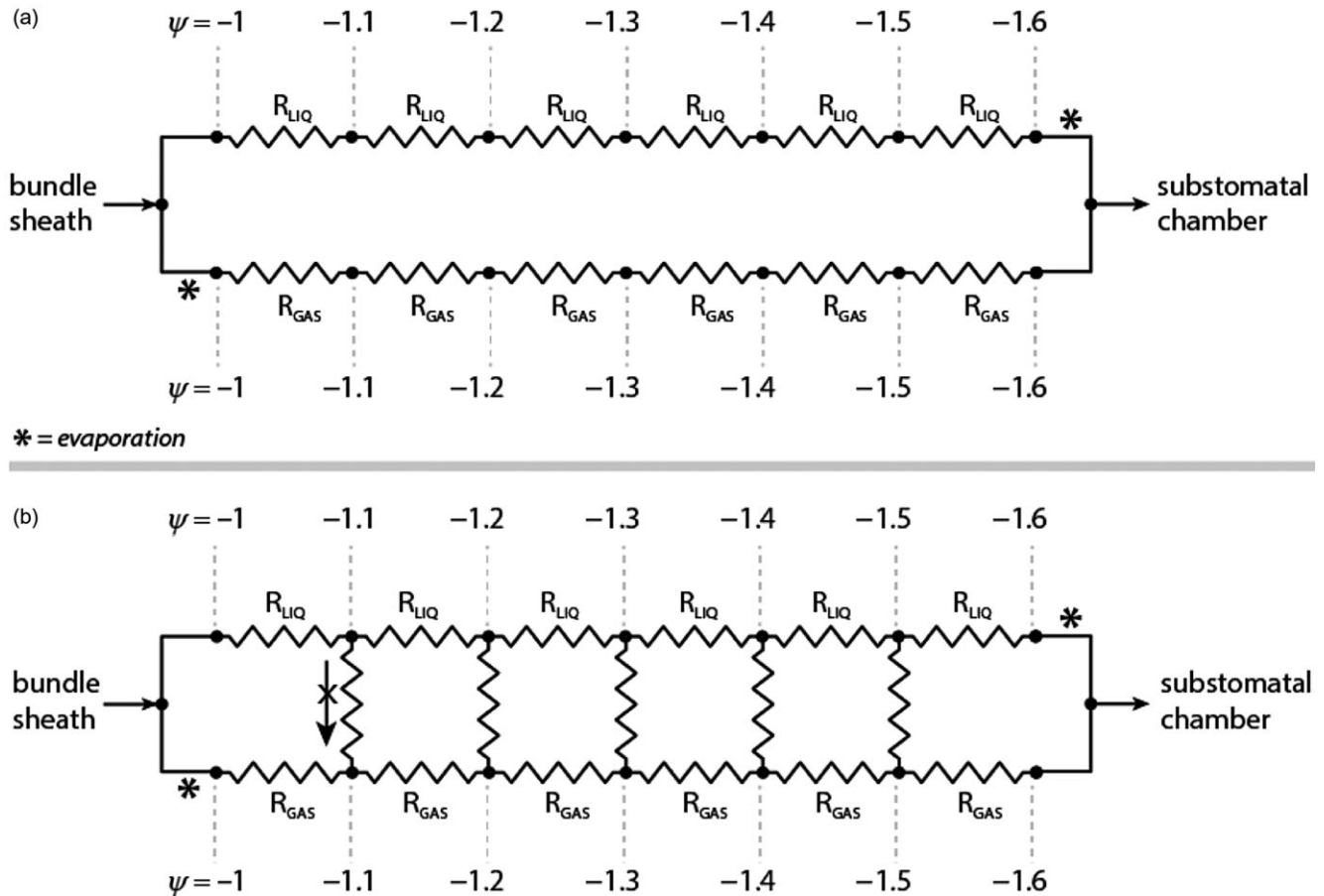


Figure 10. Diagram of parallel liquid and gas phase pathways from the bundle sheath to the substomatal chamber, either (a) excluding the possibility of evaporation at intermediate locations along the pathway, or (b) allowing it to occur by providing connections between the two pathways. If resistance accumulates in a steady fashion in each pathway, then the gradient of water potential will be the same in both pathways (e.g. from -1 to -1.6 MPa in this example). Therefore, no net flow will occur between the two pathways (arrow with 'X' in [b]), regardless of the relative magnitude of liquid and gas phase hydraulic resistances (R_{LIQ} and R_{GAS} , respectively).

mesophyll and epidermis, then 85% of evaporation will occur from the most distal sites along those pathways. Although this ignores the effect of localized reductions in temperature at the sites where water moves from a liquid phase pathway to a gas phase pathway, the important insight is the recognition that the air spaces are conduits in which water will flow, at a rate proportional to the share of total conductance contributed by those pathways. This partially reconciles the hypothesis of Boyer (1985) that much evaporation occurs from the bundle sheath, with the view that most evaporation occurs from cells lining the substomatal chamber (e.g. Tyree & Yianoulis 1980).

Factors affecting the distribution of conductance among pathways

Sensitivity analysis identified several critical parameters that strongly influence the partitioning of conductance among pathways, most notably the effective radius of hydraulic pathways for bulk flow through the apoplast (R_a) and the thickness of cell walls (t_a). R_a is poorly known, and t_a varies

by over an order of magnitude among published measurements (e.g. Nobel 1991, Rezvani Moghaddam & Wilman 1998, Hanba *et al.* 2001, Hanba *et al.* 2002, Scafaro *et al.* 2011, John *et al.* 2013). Across the range of values used for each of these parameters in this study, the apoplastic contribution to total conductance varied from 14.0% of the total (for vertical transport in spongy mesophyll, using low values for both R_a and t_a and assuming a vertical temperature gradient of 0.2 K) to 99.8% of the total (for horizontal transport in palisade mesophyll, using high values for both parameters and no temperature gradient). This highlights the importance of better knowledge of these parameters, as well as the possibility that the role of apoplastic flow may differ among species.

The effect of uniform increases in temperature also differed among pathways, with gas phase conductivity increasing much more than liquid phase conductivities. Conceptually, this is because molecular diffusion is directly driven by differences in concentration, not by differences in water potential *per se*, and the concentration gradient (Δc) corresponding to a given water potential gradient ($\Delta \psi$)

increases strongly with temperature in the gas phase but not in the liquid phase. As a result, the vapour diffusion flux per unit water potential difference (the gas phase conductivity) increases far more with temperature than does the liquid diffusion flux per unit water potential difference (the liquid phase conductivities). This does not necessarily imply that the gas phase pathway transports a greater share of water at higher temperatures, however, because it is likely that membrane conductivity P_m also increases with temperature, as found in roots (e.g. Lee *et al.* 2005, Murai-Hatano *et al.* 2008). The present study did not attempt to simulate responses of P_m to T because they are difficult to generalize and have not been adequately characterized in mesophyll cells.

Leaf hydraulic conductance (K_{leaf}) has previously been reported to increase with temperature (Sack *et al.* 2004; Cochard *et al.* 2007). These responses have been attributed to effects on aquaporins in the bundle sheath, and on the viscosity for bulk flow in the leaf xylem. The results presented here suggest that the component of K_{leaf} that resides outside of the bundle sheath should also increase strongly with temperature. This might help to explain the observation that stomata open substantially as temperature is increased while the evaporative gradient is held constant (Mott & Peak 2010): if temperature increases the conductance for water transport to the stomatal complex, then for a given transpiration rate, warming should increase water potential near the guard cells, favouring stomatal opening in the steady state (Mott *et al.* 1997; Buckley 2005). This would also explain why temperature has little effect on stomata when the evaporative gradient is negligible, as also shown by Mott & Peak (2010), because for hydraulic conductance to influence water potential, substantial water loss must be occurring. Peak & Mott (2011) explained the temperature effect by positing significant temperature gradients between the mesophyll and epidermis, combined with the hypothesis that guard cells are hydraulically sequestered from the rest of the leaf yet coupled to vapour in the adjacent air spaces. A strong temperature dependence of K_{leaf} could help to explain the results of Mott & Peak (2010) independent of the latter hypothesis, and also in situations where such gradients might be reduced – for example, in leaves whose stomata are open in darkness, so there is no light absorption to preferentially warm the centre of the leaf, or for adaxial stomata in amphistomatous leaves, in which large temperature gradients between the upper epidermis and adjacent mesophyll are less likely.

CONCLUSION

The calculations presented here suggest that the conductance for apoplastic water transport from the bundle sheath to stomata greatly exceeds that for symplastic transport, and that the gas phase conductance of the intercellular air spaces can be a substantial fraction of total conductance for vertical water transport if significant temperature gradients exist between the leaf centre and the epidermis. Further clarity on these matters awaits better knowledge of the hydraulic properties of cell membranes and cell walls in tissues outside the

bundle sheath, and of the magnitude of vertical temperature gradients within leaves.

ACKNOWLEDGMENTS

The author thanks Grace John for providing anatomical data; Lauren Sack, Christine Scoffoni, Helen Bramley, Tarryn Turnbull, Margaret Barbour, Antonio Díaz-Espejo and Kevin Simonin for helpful discussions during the preparation of this paper; and two anonymous reviewers and the Associate Editor, Professor Steve Long, for constructive comments on earlier drafts. This work was supported by funding from the US National Science Foundation (Award # 1146514), the Australian Research Council (Linkage Grant LP130101183) and the Grains Research and Development Corporation.

REFERENCES

- Agre P., Sasaki S. & Chrispeels M. (1993) Aquaporins: a family of water channel proteins. *American Journal of Physiology – Renal Physiology* **265**, F461–F461.
- Anderson C.T., Carroll A., Akhmetova L. & Somerville C. (2010) Real-time imaging of cellulose reorientation during cell wall expansion in Arabidopsis roots. *Plant Physiology* **152**, 787–796.
- Barbour M.M. & Farquhar G.D. (2004) Do pathways of water movement and leaf anatomical dimensions allow development of gradients in H₂O between veins and the sites of evaporation within leaves? *Plant, Cell & Environment* **27**, 107–121.
- Boyer J.S. (1985) Water transport. *Annual Review of Plant Physiology* **36**, 473–516.
- Brodribb T.J., Feild T.S. & Jordan G.J. (2007) Leaf maximum photosynthetic rate and venation are linked by hydraulics. *Plant Physiology* **144**, 1890–1898.
- Buckley T.N. (2005) The control of stomata by water balance (Tansley Review). *The New Phytologist* **168**, 275–292.
- Byott G.S. & Sheriff D.W. (1976) Water movement into and through *Tradescantia virginiana* (L.) leaves: II. Liquid flow pathways and evaporative sites. *Journal of Experimental Botany* **27**, 634–637.
- Canny M. (1986) Water pathways in wheat leaves. III. The passage of the mestome sheath and the function of the suberised lamellae. *Physiologia Plantarum* **66**, 637–647.
- Canny M.J. (1990) Tansley review no. 22. What becomes of the transpiration stream? *The New Phytologist* **114**, 341–368.
- Carpita N.C. & Gibeault D.M. (1993) Structural models of primary cell walls in flowering plants: consistency of molecular structure with the physical properties of the walls during growth. *The Plant Journal* **3**, 1–30.
- Chrispeels M.J. & Agre P. (1994) Aquaporins: water channel proteins of plant and animal cells. *Trends in Biochemical Sciences* **19**, 421–425.
- Cochard H., Venisse J.S., Barigah T.S., Brunel N., Herbette S., Guillot A., . . . Sakr S. (2007) Putative role of aquaporins in variable hydraulic conductance of leaves in response to light. *Plant Physiology* **143**, 122–133.
- Cosgrove D.J. (2005) Growth of the plant cell wall. *Nature Reviews. Molecular Cell Biology* **6**, 850–861.
- Evans J., Caemmerer S., Setchell B. & Hudson G. (1994) The relationship between CO₂ transfer conductance and leaf anatomy in transgenic tobacco with a reduced content of Rubisco. *Functional Plant Biology* **21**, 475–495.
- Evert R.F., Botha C.E.J. & Mierzwa R.J. (1985) Free-space marker studies on the leaf of *Zea mays* L. *Protoplasma* **126**, 62–73.
- Fahlén J. & Salmén L. (2004) Pore and matrix distribution in the fiber wall revealed by atomic force microscopy and image analysis. *Biomacromolecules* **6**, 433–438.
- Farquhar G.D. & Raschke K. (1978) On the resistance to transpiration of the sites of evaporation within the leaf. *Plant Physiology* **61**, 1000–1005.
- Fleischer A., O'Neill M.A. & Ehwald R. (1999) The pore size of non-graminaceous plant cell walls is rapidly decreased by borate ester cross-linking of the pectic polysaccharide rhamnolacturonan II. *Plant Physiology* **121**, 829–838.

- Hanba Y.T., Miyazawa S.-I., Kogami H. & Terashima I. (2001) Effects of leaf age on internal CO₂ transfer conductance and photosynthesis in tree species having different types of shoot phenology. *Functional Plant Biology* **28**, 1075–1084.
- Hanba Y.T., Kogami H. & Terashima I. (2002) The effect of growth irradiance on leaf anatomy and photosynthesis in Acer species differing in light demand. *Plant, Cell & Environment* **25**, 1021–1030.
- Holz M., Heil S.R. & Sacco A. (2000) Temperature-dependent self-diffusion coefficients of water and six selected molecular liquids for calibration in accurate ¹H NMR PFG measurements. *Physical Chemistry Chemical Physics* **2**, 4740–4742.
- John G.P., Scoffoni C. & Sack L. (2013) Allometry of cells and tissues within leaves. *American Journal of Botany* **100**, 1936–1948.
- Johnson D.L., Koplik J. & Dashen R. (1987) Theory of dynamic permeability and tortuosity in fluid-saturated porous media. *Journal of Fluid Mechanics* **176**, 379–402.
- Kaiser H. & Legner N. (2007) Localization of mechanisms involved in hydropassive and hydroactive stomatal responses of *Sambucus nigra* to dry air. *Plant Physiology* **143**, 1068–1077.
- Kennedy C., Šturcová A., Jarvis M. & Wess T. (2007) Hydration effects on spacing of primary-wall cellulose microfibrils: a small angle X-ray scattering study. *Cellulose* **14**, 401–408.
- Koponen A., Kataja M. & Timonen J. (1996) Tortuous flow in porous media. *Physical Review E* **54**, 406–410.
- Lee S.H., Chung G.C. & Steudle E. (2005) Gating of aquaporins by low temperature in roots of chilling-sensitive cucumber and chilling-tolerant figleaf gourd. *Journal of Experimental Botany* **56**, 985–995.
- McCann M.C., Wells B. & Roberts K. (1990) Direct visualization of cross-links in the primary plant-cell wall. *Journal of Cell Science* **96**, 323–334.
- Massman W.J. (1998) A review of the molecular diffusivities of H₂O, CO₂, CH₄, CO, O₃, SO₂, NH₃, N₂O, NO, and NO₂ in air, O₂ and N₂ near STP. *Atmospheric Environment* **32**, 1111–1127.
- Meziane D. & Shipley B. (1999) Interacting determinants of specific leaf area in 22 herbaceous species: effects of irradiance and nutrient availability. *Plant, Cell & Environment* **22**, 447–459.
- Morillon R. & Chrispeels M.J. (2001) The role of ABA and the transpiration stream in the regulation of the osmotic water permeability of leaf cells. *Proceedings of the National Academy of Sciences* **98**, 14138–14143.
- Mott K.A. & Peak D. (2010) Stomatal responses to humidity and temperature in darkness. *Plant, Cell & Environment* **33**, 1084–1090.
- Mott K.A., Denne F. & Powell J. (1997) Interactions among stomatal in response to perturbations in humidity. *Plant, Cell and Environment* **20**, 1098–1107.
- Murai-Hatano M., Kuwagata T., Sakurai J., Nonami H., Ahamed A., Nagasuga K., . . . Okada M. (2008) Effect of low root temperature on hydraulic conductivity of rice plants and the possible role of aquaporins. *Plant and Cell Physiology* **49**, 1294–1305.
- Nobel P.S. (1991) *Physicochemical and Environmental Plant Physiology*, Academic Press, London, UK.
- Peak D. & Mott K.A. (2011) A new, vapour-phase mechanism for stomatal responses to humidity and temperature. *Plant, Cell & Environment* **34**, 162–178.
- Pieruschka R., Huber G. & Berry J.A. (2010) Control of transpiration by radiation. *Proceedings of the National Academy of Sciences* **107**, 13372–13377.
- Rezvani Moghaddam P. & Wilman D. (1998) Cell wall thickness and cell dimensions in plant parts of eight forage species. *The Journal of Agricultural Science* **131**, 59–67.
- Rockwell F., Holbrook N.M. & Stroock A.D. (2014) The competition between liquid and vapor transport in transpiring leaves. *Plant Physiology* **164**, 1741–1758. doi: <http://dx.doi.org/10.1104/pp.1114.236323>.
- Sack L., Streeter C.M. & Holbrook N.M. (2004) Hydraulic analysis of water flow through leaves of sugar maple and red oak. *Plant Physiology* **134**, 1824–1833.
- Sack L., Tyree M.T. & Holbrook N.M. (2005) Leaf hydraulic architecture correlates with regeneration irradiance in tropical rainforest trees. *The New Phytologist* **167**, 403–413.
- Scafaro A.P., Von Caemmerer S., Evans J.R. & Atwell B.J. (2011) Temperature response of mesophyll conductance in cultivated and wild *Oryza* species with contrasting mesophyll cell wall thickness. *Plant, Cell & Environment* **34**, 1999–2008.
- Scoffoni C., Pou A., Aasamaa K. & Sack L. (2008) The rapid light response of leaf hydraulic conductance: new evidence from two experimental methods. *Plant, Cell and Environment* **31**, 1803–1812.
- Shatil-Cohen A., Attia Z. & Moshelion M. (2011) Bundle-sheath cell regulation of xylem-mesophyll water transport via aquaporins under drought stress: a target of xylem-borne ABA? *The Plant Journal* **67**, 72–80.
- Strugger S. (1943) Der aufsteigende Saftstrom in der Pflanze. *Naturwissenschaften* **31**, 181–191.
- Tanton T. & Crowdy S. (1972) Water pathways in higher plants III. The transpiration stream within leaves. *Journal of Experimental Botany* **23**, 619–625.
- Terashima I., Hanba Y.T., Tazoe Y., Vyas P. & Yano S. (2006) Irradiance and phenotype: comparative eco-development of sun and shade leaves in relation to photosynthetic CO₂ diffusion. *Journal of Experimental Botany* **57**, 343–354.
- Thomas L.H., Forsyth V.T., Šturcová A., Kennedy C.J., May R.P., Altaner C.M., . . . Jarvis M.C. (2013) Structure of cellulose microfibrils in primary cell walls from collenchyma. *Plant Physiology* **161**, 465–476.
- Tyree M., Cruiziat P., Benis M., LoGullo M. & Salleo S. (1981) The kinetics of rehydration of detached sunflower leaves from different initial water deficits. *Plant, Cell & Environment* **4**, 309–317.
- Tyree M., Sobrado M.A., Stratton L. & Becker P. (1999) Diversity of hydraulic conductance in leaves of temperate and tropical species: possible causes and consequences. *Journal of Tropical Forest Science* **11**, 47–60.
- Tyree M.T. & Yianoulis P. (1980) The site of water evaporation from sub-stomatal cavities, liquid path resistances and hydroactive stomatal closure. *Annals of Botany* **45**, 175–193.
- World Meteorological Organization (2008) *Guide to Meteorological Instruments and Methods of Observation*, WMO, Geneva, Switzerland.
- Zwieniecki M.A., Brodribb T.J. & Holbrook N.M. (2007) Hydraulic design of leaves: insights from rehydration kinetics. *Plant, Cell and Environment* **30**, 910–921.

Received 6 March 2014; received in revised form 5 May 2014; accepted for publication 7 May 2014

SUPPORTING INFORMATION

Additional Supporting Information may be found in the online version of this article at the publisher's web-site:

Table S1. Spreadsheet demonstrating the calculations shown in this paper.

APPENDIX 1. CONDUCTANCES THROUGH EACH TISSUE TYPE AND FLOW DIRECTION

This Appendix will derive estimates for the relative flow areas of each pathway, in both horizontal and vertical directions and for each tissue type separately, in order to create expressions for the conductances of each pathway. These areas will be estimated using the conceptual model shown in Fig. 1, in which a leaf consists of epidermal, palisade and spongy layers whose thicknesses are fractions z_E , z_P and z_S of total leaf thickness. Palisade cells will be modelled as cylinders with spherical ends (capsules) with height eight times the radius r_P , and spongy cells will be modelled as spheres with radius r_S (e.g. Nobel 1991, Evans *et al.* 1994). Epidermal cells will be modelled as cubes with length x_E . In what follows, the subscripts H and V will be used to denote horizontal and vertical transport, respectively.

Horizontal liquid phase transport (parallel to the epidermis)

The area available for horizontal gas phase transport through the palisade is $z_P p_P A_H$, where p_P is the porosity of the palisade tissue and A_H is the total area of a transverse leaf section. For gas transport through the spongy tissue, the area

is $z_S p_S A_H$. The total cross-sectional area of epidermal cells is $A_{H,E} = z_E A_H$. The cross-sectional areas of palisade and spongy mesophyll cells ($A_{H,P}$ and $A_{H,S}$, respectively) are $(1 - p_P) z_P A_H$ and $(1 - p_S) z_S A_H$, respectively.

The projected areas $A_{H,E}$, $A_{H,S}$ and $A_{H,P}$ will now be related to the actual areas relevant to transmembrane, transcellular and apoplastic flow in the horizontal direction. A large fraction of mesophyll surface area is not available for liquid phase symplastic water flow between cells because it adjoins air spaces rather than other cells and is typically appressed with chloroplasts (e.g. Evans *et al.* 1994, Terashima *et al.* 2006). The remaining area is a fraction, f_c , of mesophyll surface area. The ratio of cell surface area to horizontal projected cross-sectional area is easily shown to be 3.32 for palisade cells and 4 for spongy cells with the geometry assumed here and shown in Fig. 1. Because water moving away from the bundle sheath encounters only half of this surface area (the other half is at the far side of the cell), the area for transmembrane flow in the horizontal direction is $1.66 f_c A_{H,P}$ for palisade cells and $2 f_c A_{H,S}$ for spongy cells. For epidermal cells, this area is simply $A_{H,E}$. The areas for transcellular flow are simply the projected cross-sectional areas ($A_{H,P}$, $A_{H,S}$ and $A_{H,E}$); in practice, cellular contents will impede diffusion to some degree, so these values most likely overestimate the effective transcellular flow areas.

The area for apoplastic flow is approximately equal to the product of cell wall thickness, t_a , and cell circumference, and the latter, in turn, can easily be expressed in relation to projected cross-sectional area. It is easily shown that the ratios of circumference to cross-sectional area are $4/x_E$, $1.21/r_P$ and $2/r_S$ for epidermal, palisade and spongy cells, respectively, using the cell geometries assumed here and shown in Fig. 1. Thus, the apoplastic flow areas for epidermal, palisade and spongy cells are $4A_{H,E}t_a/x_E$, $1.21A_{H,P}t_a/r_P$ and $2A_{H,S}t_a/r_S$, respectively.

These areas will now be applied to the conductivities derived in the main text. The conductance for horizontal entry into a single cell of tissue type j ($j = P, S$ and E for palisade, spongy and epidermal cells, respectively), $K_{mH,j}$, is the product of membrane conductivity k_m and transmembrane flow area, or

$$K_{mH,P} = 1.66 f_c A_{H,P} k_m, \quad (\text{A1})$$

$$K_{mH,S} = 2 f_c A_{H,S} k_m \quad (\text{A2})$$

and

$$K_{mH,E} = A_{H,E} k_m. \quad (\text{A3})$$

The conductance for horizontal flow across a single cell of type j , $K_{ch,j}$, is the product of transcellular conductivity k_c and transcellular flow area, or

$$K_{ch,P} = A_{H,P} k_c, \quad (\text{A4})$$

$$K_{ch,S} = A_{H,S} k_c \quad (\text{A5})$$

and

$$K_{ch,E} = A_{H,E} k_c. \quad (\text{A6})$$

Finally, the conductance for horizontal apoplastic flow around a single cell of type j , $K_{ah,j}$, is the product of apoplastic conductivity and apoplastic flow area, or

$$K_{ah,P} = 1.21 A_{H,P} t_a k_a / r_P, \quad (\text{A7})$$

$$K_{ah,S} = 2 A_{H,S} t_a k_a / r_S \quad (\text{A8})$$

and

$$K_{ah,E} = 4 A_{H,E} t_a k_a / x_E. \quad (\text{A9})$$

Horizontal gas phase transport

The areas for horizontal gas diffusion through the palisade and spongy mesophyll were derived earlier as $z_P p_P A_H$ and $z_S p_S A_H$, respectively, so the horizontal gas phase conductances for palisade and spongy tissues are

$$K_{gasH,P} = z_P p_P A_H k_g \quad (\text{A10})$$

and

$$K_{gasH,S} = z_S p_S A_H k_g. \quad (\text{A11})$$

Vertical liquid phase transport

Epidermal cells do not participate in vertical transport, so it is only necessary to compute areas for vertical transport through palisade and spongy cells. The calculations below assume that the fraction of area occupied by airspace in a paradermal plane (normal to the vertical flow axis) is equal to the tissue porosity, which implies that the projected cross-sectional areas of palisade and spongy cells in this plane are $A_{V,P} = (1 - p_P) A_V$ and $A_{V,S} = (1 - p_S) A_V$, where A_V is the total area of a paradermal section. Using the cell geometries shown in Fig. 1, and following the logic presented earlier in the Horizontal liquid phase transport section, the area for transmembrane flow vertically into a single cell is $2 f_c A_{V,P}$ for palisade cells and $2 f_c A_{V,S}$ for spongy cells. The transcellular flow areas are $A_{V,P}$ and $A_{V,S}$, respectively. The apoplastic areas are $2 A_{V,P} t_a / r_P$ and $2 A_{V,S} t_a / r_S$ for palisade and spongy cells, respectively. Thus, the conductances for vertical transmembrane flow into a single cell of type j , $K_{mV,j}$, are

$$K_{mV,P} = 2 f_c A_{V,P} k_m \quad (\text{A12})$$

and

$$K_{mV,S} = 2 f_c A_{V,S} k_m. \quad (\text{A13})$$

The conductances for vertical transcellular flow across a single cell of type j , $K_{cv,j}$, are

$$K_{cv,P} = A_{V,P} k_c \quad (\text{A14})$$

and

$$K_{cv,S} = A_{V,S} k_c. \quad (\text{A15})$$

The conductances for vertical apoplastic flow around a single cell of type j , $K_{av,j}$, are

$$K_{aV,P} = 2A_{V,P}t_a k_a / r_P \quad (\text{A16})$$

and

$$K_{aV,S} = 2A_{V,S}t_a k_a / r_S \quad (\text{A17})$$

Vertical gas phase transport

The areas available for vertical gas transport through the palisade and spongy tissues are $p_P \cdot A_V$ and $p_S \cdot A_V$, respectively, so the conductances for vertical gas transport through these tissues are

$$K_{gasV,P} = p_P A_V k_g \quad (\text{A18})$$

and

$$K_{gasV,S} = p_S A_V k_g \quad (\text{A19})$$

Scaling from single cells to whole paths

The liquid phase conductances derived earlier apply to single cells, and for symplastic flow they apply to different components of the flow pathway within each cell: that is through a membrane and across the cell. This section will scale these conductances up to whole-path values for each cell type and flow direction. The total symplastic conductance across a single cell of type j is $(2/K_{mHj} + 1/K_{cHj})^{-1}$ for horizontal flow or $(2/K_{mVj} + 1/K_{cVj})^{-1}$ for vertical flow. This is because two membranes and one cellular interior must be crossed in series. The total symplastic conductance of the entire liquid phase pathway for cell type j is $K_{symHj} = n_{Hj}^{-1} \cdot (2/K_{mHj} + 1/K_{cHj})^{-1}$ for horizontal flow or $K_{symVj} = n_{Vj}^{-1} \cdot (2/K_{mVj} + 1/K_{cVj})^{-1}$ for vertical flow, where n_{Hj} and n_{Vj} are the numbers of cells of type j encountered along the horizontal and vertical flow paths, respectively. The apoplastic conductance along a single cell of type j is simply K_{aHj} (horizontal) or K_{aVj} (vertical), and the total apoplastic conductance of the entire liquid phase pathway for cell type j is K_{aHj}/n_{Hj} (horizontal) or K_{aVj}/n_{Vj} (vertical).

The number of cells of each type encountered in the horizontal flow path, n_{Hj} , can be calculated from cell dimensions and the total horizontal distance along the liquid phase flow axis, l_{LH} : $n_{H,E} \cdot x_E = n_{H,P} \cdot 2r_P = n_{H,S} \cdot 2r_S = l_{LH}$, so $n_{H,E} = l_{LH}/x_E$, $n_{H,P} = l_{LH}/2r_P$ and $n_{H,S} = l_{LH}/2r_S$. Similarly, $n_{V,P}$ is the vertical liquid phase flow pathlength in palisade ($l_{LV,P}$) divided by the height of a palisade cell ($8r_P$), or $n_{V,P} = l_{LV,P}/8r_P$; for spongy cells, $n_{V,S}$ is the vertical liquid phase flow pathlength in spongy mesophyll ($l_{LV,S}$) divided by the height of a spongy cell ($2r_S$), or $n_{V,S} = l_{LV,S}/2r_S$.

APPENDIX 2. ESTIMATION OF PARAMETER VALUES

This Appendix will estimate nominal values and ranges for the parameters used to compute the conductivities derived in the main text, and the conductances whose calculation is

described in Appendix 1. Values and ranges for parameters that varied in sensitivity analyses are summarized in Table 2.

Physical parameters

The gas constant R is $8.3144621 \text{ Pa m}^3 \text{ mol}^{-1} \text{ K}^{-1}$. The molar volume of liquid water, V_w , is $1.8 \cdot 10^{-5} \text{ m}^3 \text{ mol}^{-1}$. Saturation water vapour pressure, p_{sat} , is a function of temperature: $p_{sat} = 611.2 \cdot \exp(17.62 \cdot T_c / (243.12 + T_c)) \text{ Pa}$, where T_c is in degrees Celsius (World Meteorological Organization 2008). The self-diffusion coefficient of liquid water in water, D_{ww} , is $1.635 \cdot 10^{-8} \cdot (T/215.05 - 1)^{2.063} \text{ m}^2 \text{ s}^{-1}$ (Holz *et al.* 2000), and the diffusion coefficient of water vapour in air, D_{wa} , is $2.178 \cdot 10^{-5} \cdot (T/273.15)^{1.81} \text{ m}^2 \text{ s}^{-1}$ (Massman 1998), where T is in kelvins. A leaf temperature of $25 \text{ }^\circ\text{C}$ was used unless otherwise noted.

Ratio of gas phase pathlength to liquid phase pathlength

This ratio cannot be measured directly from anatomical dimensions, because the actual paths taken by vapour and liquid water cannot be deduced solely from geometrical considerations. One approach to estimating this ratio is to estimate the ratio of the tortuosities of each pathway (tortuosity is the ratio of actual mean pathlength to the minimum straight-line pathlength). Studies on the tortuosity of flow paths in porous materials have generally concluded that tortuosity increases strongly as porosity decreases (e.g. Johnson *et al.* 1987, Koponen *et al.* 1996), so a reasonable range for the ratio of gas and liquid phase pathlengths can be estimated using models of the tortuosity–porosity relationship applied to measured tissue porosities. One widely cited model (Koponen *et al.* 1996) suggests tortuosity = $1 + 0.8 \cdot (1 - \text{porosity})$; applied to the porosity ranges given earlier, this suggests a range of pathlength ratios (gas/liquid) from 1.12 to 1.65 for palisade and from 0.86 to 1.30 for spongy tissues, with ratios of 1.43 and 1.13, respectively, corresponding to the mean values of p_P and p_S given earlier. Nominal values for the ratio of gas to liquid phase pathlength in palisade and spongy tissues were thus taken as 1.43 and 1.13, respectively. To accommodate uncertainty in the tortuosity/porosity relationship, the ranges given above were doubled (i.e. 0.90–1.96 for palisade and 0.69–1.57 for spongy mesophyll). Gas phase pathlengths in both horizontal and vertical directions for spongy mesophyll, and for the horizontal direction in palisade mesophyll, were computed in this manner. However, because vertical gas pathways in palisade are not tortuous due to the parallel nature of palisade cells, the ratio of liquid to gas phase pathlengths was assumed to be 1.0 for vertical pathways in the palisade.

Cell water permeability, P_m

Estimates of P_m vary widely, and the distribution of P_m among mesophyll cells in a given leaf is commonly reported to be bimodal. For example, Morillon & Chrispeels (2001) found modes at $P_m \approx 5$ and $160 \cdot 10^{-6} \text{ m s}^{-1}$ with an overall mean of $69 \cdot 10^{-6}$ and similar cell numbers in each mode. Shtil-Cohen *et al.* (2011) found modes at $P_m = 5.4 \cdot 10^{-6} \text{ m s}^{-1}$

and $58 \cdot 10^{-6} \text{ m s}^{-1}$, with 90% of cells in the low- P_m mode and an overall mean of $10.7 \cdot 10^{-6} \text{ m s}^{-1}$. In the present study, $10 \cdot 10^{-6}$ and $70 \cdot 10^{-6}$ were used as low and high values, respectively, for average P_m among mesophyll cells in a leaf, with a nominal value in the middle of this range, at $40 \cdot 10^{-6} \text{ m s}^{-1}$.

Water-conducting fraction of mesophyll surface area, f_c

The fraction, f_c , of mesophyll surface area that is connected to adjacent cells averaged 0.18 among seven annual species and 0.37 among 25 tree species in the metadata compiled from the literature by Terashima *et al.* (2006). In the present study, 0.15 and 0.40 were used as lower and upper values, respectively, and 0.275 was used as the nominal value.

Cell wall thickness, t_a

Mesophyll and epidermal cell walls are typically between 0.2 and $0.4 \cdot 10^{-6} \text{ m}$ in thickness (e.g. Nobel 1991, Rezvani Moghaddam & Wilman 1998, Hanba *et al.* 2001, Hanba *et al.* 2002, Scafaro *et al.* 2011). This range was used in the present study, with a nominal value of $0.3 \cdot 10^{-6} \text{ m}$. However, a recent study by John *et al.* (2013) of 14 species found much larger values for cell wall thickness, averaging $1.4 \cdot 10^{-6} \text{ m}$ and ranging from 0.5 to $2.5 \cdot 10^{-6} \text{ m}$. An alternative set of calculations was therefore performed using the latter mean and range.

Cell radii, r_p and r_s

Mesophyll cell size varies widely and cannot easily be generalized. John *et al.* (2013) reported mean transverse areas of spongy and mesophyll cells across 14 species, ranging from approximately 100 to $1100 \mu\text{m}^2$ for spongy cells and 200 to $1400 \mu\text{m}^2$ for palisade cells. For the cell models shown in Fig. 1, this implies radius ranges of $r_s = 5.6$ to $18.7 \cdot 10^{-6} \text{ m}$ for spongy cells and $r_p = 3.6$ to $9.6 \cdot 10^{-6} \text{ m}$ for palisade cells. Based on these values, the present study used $5 \cdot 10^{-6}$ – $19 \cdot 10^{-6} \text{ m}$ as the range for spongy cells and $3 \cdot 10^{-6}$ – $10 \cdot 10^{-6} \text{ m}$ for palisade cells, with nominal values taken as the middle of these ranges ($r_s = 12 \cdot 10^{-6} \text{ m}$ and $r_p = 6.5 \cdot 10^{-6} \text{ m}$).

Epidermal cell size, x_E

Like mesophyll cells, epidermal cells vary widely in size. John *et al.* (2013) reported mean transverse areas ranging from approximately 120 to $1850 \mu\text{m}^2$, giving a cell length range of 11 to $43 \cdot 10^{-6} \text{ m}$ for cubical cells. The present study used this range for x_E , and the middle of the range ($27 \cdot 10^{-6} \text{ m}$) as the nominal value of x_E .

Palisade and spongy mesophyll tissue porosities, p_p and p_s

In the survey of 14 species by John *et al.* (2013), the authors found mean $p_p = 0.19$ with a range of 0.07 to 0.40, and mean $p_s = 0.39$ with a range of 0.27 to 0.63 (John *et al.*, unpublished

data). These means were used in the present study as nominal values, and the ranges were used as upper and lower limits.

Ratio of apoplastic to transcellular pathlength, y

Water moving around a cell that is circular in cross-section with radius r will have to travel half of the cell's circumference, or πr , whereas water moving directly across the cell will only have to travel a distance $2r$, which suggests $y = \pi/2$ for horizontal flow around palisade or spongy mesophyll cells. However, connections between mesophyll cells will reduce the effective cell circumference by a factor $1 - f_c$ (where f_c is the fraction of mesophyll cell surface area that is connected to other mesophyll cells), so $y = (1 - f_c)\pi/2$ for horizontal flow around mesophyll cells. For vertical flow in palisade cells, the transcellular pathlength is the cell height, or $8r_p$, whereas the apoplastic pathlength is $(1 - f_c)\pi r_p + 6r_p$; thus $y = ((1 - f_c)\pi + 6)/8$ for vertical flow around palisade cells. For epidermal cells, $y = 1$.

Tissue thickness fractions, z_E , z_p and z_s

The mean epidermal fraction, z_E , of total leaf thickness among 22 herbaceous species grown at high light and nutrient supplementation in a study by Meziane & Shipley (1999) was 0.19, with lower and upper limits of 0.05 and 0.38; the present study used these as the nominal value, lower and upper limit, respectively. The mean ratio of palisade to spongy thickness (z_p/z_s) varied from 0.85 to 0.69 in a survey of 14 species by John *et al.* (2013). The present study used a nominal value of 0.75 and a range of 0.5 to 2.0 for z_p/z_s , and calculated z_s and z_p thus: $z_s = 1 - z_E - z_p = 1 - z_E - (z_p/z_s)z_s$, which gives $z_s = (1 - z_E)/(1 + z_p/z_s)$ and $z_p = 1 - z_E - z_s$.

Poiseuille radius of cell wall bulk flow pathways, R_a

Cellulose microfibrils in primary cell walls are around 3 nm ($3 \cdot 10^{-9} \text{ m}$) in diameter (Thomas *et al.* 2013) and are spaced approximately 20–40 nm apart (McCann *et al.* 1990). However, much of the space between microfibrils is occupied by pectins and by cross-linking molecules such as xyloglucans (Carpita & Gibeau 1993; Cosgrove 2005). Studies on primary walls in collenchyma suggest much closer spacing on the order of 5 nm (Kennedy *et al.* 2007), although this may indicate aggregation of microfibrils into larger-order structures (Anderson *et al.* 2010; Thomas *et al.* 2013), as is known to occur in wood fibres, where microfibrils aggregate into bundles of roughly 15–20 nm in diameter (Fahlén & Salmén 2004). The effective pore diameter for movement of molecules across the primary cell wall (into or out of cells – i.e. perpendicular to the main direction of apoplastic flow in the transpiration stream) is roughly 3 nm and this is highly dependent on pectin content (Fleischer *et al.* 1999). Together, these results suggest that the effective pore diameter for water flow through the primary wall matrix is between 3 and 20 nm, and is more likely near the low end of this range. The present study used a nominal value of $6 \cdot 10^{-9} \text{ m}$ for the

diameter (which gives $R_a = 3 \cdot 10^{-9}$ m), and lower and upper limits of $1.5 \cdot 10^{-9}$ m and $10 \cdot 10^{-9}$ m for R_a .

Effective cell wall porosity, p_a/τ_a

This parameter is unknown, but is often assumed to be approximately 0.3 (e.g. Nobel 1991, Evans *et al.* 1994). Terashima *et al.* (2006) argued that a value of 0.1 was more likely, on the basis that wall thickness would have too little impact on mesophyll CO₂ conductance to explain observed differences in this conductance with wall thickness if p_a/τ_a were 0.3. Scafaro *et al.* (2011) suggested a value of 0.2 was consistent with their observations of effects of wall thickness and other properties on mesophyll conductance. It is possible, however, that the value of p_a/τ_a relevant to flow along the walls, rather than across them, is higher, because unlike flow across walls, flow along walls will encounter at least some paths that are approximately parallel to microfibrils. To account for this uncertainty, the present study used a nominal value of 0.2 for p_a/τ_a , but a wider range of 0.1 to 0.5 for sensitivity analysis.

Total horizontal and vertical liquid phase pathlengths (l_{LH} , $l_{LV,P}$, $l_{LV,S}$) and total horizontal and vertical flow areas (A_H , A_V)

These parameters do not influence the proportions of conductance in each pathway for a given tissue and flow direction, so they are arbitrary for the purposes of the present study and are included only for the sake of completeness. The present study used values of $1 \cdot 10^{-4}$ m for each of these pathlengths and $5 \cdot 10^{-8}$ m² for each area.

APPENDIX 3. MOLAR CONDUCTIVITY OF GAS PHASE TRANSPORT WITHIN LEAVES UNDER ANISOTHERMAL CONDITIONS

In the main text, the molar conductivity for gas phase transport within the leaf was derived by beginning with Fick's first law of diffusion:

$$J_g = D \frac{dc}{dx} \approx \frac{D_{wa}}{l_g} \Delta c, \quad (\text{A20})$$

where J_g is the water vapour flux (subscript g for gas phase) ($\text{mol m}^{-2} \text{s}^{-1}$), D_{wa} is the molecular diffusivity of water vapour in air ($\text{m}^2 \text{s}^{-1}$), l_g is the length of the gas phase flow path through the intercellular spaces (m) and Δc is the difference in water vapour concentration (mol m^{-3}) across that pathway. The molar conductivity of this pathway, k'_g , is J_g divided by the water potential difference across the pathway, $\Delta\psi$, or

$$k'_g = \frac{D_{wa}}{l_g} \frac{\Delta c}{\Delta\psi}, \quad (\text{A21})$$

The main text noted that water potential ψ is related to water vapour mole fraction (w , mol mol^{-1}) by $\psi \approx (RT/V_w)(w/w_s - 1)$, where w_s is the saturation water vapour mole fraction

of air at a temperature T (kelvins), and that w/w_s in turn is equal to the ratio of c/c_s , where c and c_s are water vapour concentration under actual and saturated conditions, respectively. This can be rearranged to give c in terms of ψ and c_s :

$$c \approx c_s \left(\frac{\psi V_w}{RT} + 1 \right). \quad (\text{A22})$$

The concentration difference across the gas phase pathway can be expressed as

$$\Delta c = c_1 - c_2 = \left(\frac{c_{s1} \psi_1 V_w}{RT_1} - \frac{c_{s2} \psi_2 V_w}{RT_2} \right) + (c_{s1} - c_{s2}), \quad (\text{A23})$$

where the subscripts 1 and 2 denote the beginning and end-points of the pathway, respectively, and c_s is the value of c at saturation. This can be rearranged to give

$$\Delta c = \frac{c_{s1} V_w}{RT_1} \Delta\psi + \frac{V_w}{RT_1} \psi_2 \left(c_{s1} - c_{s2} \frac{T_1}{T_2} \right) + (c_{s1} - c_{s2}), \quad (\text{A24})$$

where $\Delta\psi = \psi_1 - \psi_2$. Dividing through by $\Delta\psi$ gives

$$\frac{\Delta c}{\Delta\psi} = \frac{c_{s1} V_w}{RT_1} + \frac{V_w}{RT_1} \frac{\psi_2}{\Delta\psi} \left(c_{s1} - c_{s2} \frac{T_1}{T_2} \right) + \frac{1}{\Delta\psi} (c_{s1} - c_{s2}). \quad (\text{A25})$$

Note that $T_1/T_2 = (T_2 + \Delta T)/T_2 = 1 + \Delta T/T_2$. Simulations by Rockwell *et al.* (2014) indicated that the vertical temperature gradient between the vascular plane and epidermis is likely on the order of 0.1 K, so $\Delta T \ll T_2$ and thus $T_1/T_2 \approx 1$ in the term in parentheses in Eqn A25. Applying this to Eqn A25 and rearranging terms gives

$$\frac{\Delta c}{\Delta\psi} = \frac{c_{s1} V_w}{RT_1} + \left(\frac{c_{s1} - c_{s2}}{\Delta\psi} \right) \left(\frac{\psi_2 V_w}{RT_1} + 1 \right). \quad (\text{A26})$$

Using the gas law ($c = p/RT$) to write c_{s1} and c_{s2} in terms of the corresponding saturation vapour pressures, $p_{\text{sat}1}$ and $p_{\text{sat}2}$, respectively, we have

$$\frac{\Delta c}{\Delta\psi} = \frac{p_{\text{sat}1} V_w}{(RT_1)^2} + \frac{1}{R \Delta\psi} \left(\frac{\psi_2 V_w}{RT_1} + 1 \right) \left(\frac{p_{\text{sat}1}}{T_1} - \frac{p_{\text{sat}2}}{T_2} \right). \quad (\text{A27})$$

Finally, applying Eqn A27 to Eqn A21 gives

$$k'_g = \frac{D_{wa} p_{\text{sat}1} V_w}{l_g (RT_1)^2} + \frac{D_{wa}}{l_g R \Delta\psi} \left(\frac{\psi_2 V_w}{RT_1} + 1 \right) \left(\frac{p_{\text{sat}1}}{T_1} - \frac{p_{\text{sat}2}}{T_2} \right). \quad (\text{A28})$$

The first term on the right hand side of Eqn A28 is the isothermal molar conductivity to gas diffusion in the intercellular air spaces, k_g (Eqn 14 in the main text). Thus, Eqn A28 is equivalent to Eqn 15 in the main text. The present study only considered vertical, not horizontal temperature gradients. This is because there is strong reason to suppose illuminated leaves will be warmer near the leaf centre (where light is absorbed by mesophyll tissue) than near the epidermis; by contrast, any assumptions regarding horizontal temperature gradients would be conflated with assumptions regarding the distribution of evaporating sites, which are poorly known.